Segmented copolymers with polyesteramide units of uniform length: structure analysis

P. F. van Hutten, R. M. Mangnus and R. J. Gaymans*
Department of Chemical Technology, University of Twente, PO Box 217, 7500 AE Enschede, The Netherlands
(Received 18 January 1993)

Segmented poly(ether esteramide) copolymers with short ($M = 382$) partially aromatic esteramide units of uniform length and segments of poly(tetramethylene oxide) (PTMO) have beem synthesized in the melt. The polymers show phase separation into two or three phases. The influence of the PTMO segment length on the following properties was studied: the T_g of the amorphous phase, the T_m of the crystalline PTMO and the melting and crystallization behaviour of the uniform polyesteramide units. Volume fraction and density of each phase were determined. The polyesteramide units crystallize in lamellar structures; their sizes were studied using WAXD and SAXS. The polymers were melt processed and their mechanical properties were investigated using dynamic mechanical thermal analysis (d.m.t.a.) and tensile tests. Polyesteramide crystallinity, crystalline structure and crystallite size were found to be almost independent of PTMO segment length. The decrease in hard-segment melting temperature with increasing PTMO segment length is explained as being due to a 'solvent' effect of the soft phase. The copolymers crystallize very fast, and the modulus in the rubber region is essentially independent of temperature. The copolymers with long PTMO segments ($M = 2000$ and 2900) have a low glass transition temperature (−65°C); the materials are very soft and have an elongation at break of over 1000%. The copolymer with the shortest PTMO segments ($M = 250$) has a glass transition temperature of 43°C and the material is hard at room temperature.

(Keywords: segmented copolymers; poly(tetramethylene oxide); polyesteramide)

INTRODUCTION

The segmented block copolymers are an interesting class of thermoplastic materials[1]. These materials are built up from two types of segments, which alternate many times in the polymer chains. One of the segments (the 'soft' block) consists of chain elements with a low T_g. The other (the 'hard' block) consists of elements which can aggregate or crystallize to form rigid physical crosslinks, thereby giving the material mechanical properties resembling those of crosslinked elastomers.

When crystalline hard blocks are employed, the material phase separates as a crystalline phase, consisting of pure hard block, and an amorphous phase, consisting of soft block and uncrystallized hard block. The amorphous phase gives the material its elastomeric properties, while the crystalline phase gives the material its dimensional stability. Above the melting point of the crystalline phase the material is a liquid and melt processing is possible. Upon cooling, the phase separation is restored by crystallization of the hard block and the material regains its elastomeric properties. Since the amorphous phase and the crystalline phase have a different chemical structure, the T_g/T_m ratio can have a value lower than 2/3, which is common for pure semicrystalline thermoplastics.

* To whom correspondence should be addressed

0032-3861/93/204193-10

The best known types of hard blocks in segmented block copolymers are polyurethanes, poly(butylene terephthalate) (PBT) or polyamides, with polyethers or aliphatic polyesters acting as the soft blocks[2–4]. Phase separation by crystallization and the crystalline phase structure are crucial for these materials. The rate of crystallization of the hard block is comparable to that of its homopolymer, and with decreasing hard block length crystallization becomes more difficult. For PBT hard blocks the minimum length required for hard block crystallization to occur is four repeating units[2], while for nylon-46 it is two repeating units[5]. When this critical block length is approached the hard block crystallinity also decreases. The hard block melting temperature becomes lower with decreasing hard block length, which has been explained as being caused by the smaller lamellar thickness of the crystallites[6].

In most segmented block copolymers, the crystallizable segment has a broad block length distribution. Polyurethanes with a uniform hard block length have been studied[7,8], and these materials were found to have a better microphase separation, a higher modulus, a higher elongation at break and a lower drop in modulus with temperature in the rubber region. In these materials the hard block melting temperature also decreases with decreasing block length, and very short blocks with only two urethane groups phase separate only with difficulty[9,10].

In another article we have reported the synthesis of segmented copolymers containing short poyesteramide hard units of uniform length and polyether soft segments[11]. These copolymers were synthesized from *N,N'*-bis(*p*-carbomethoxybenzoyl) butane diamine (T4T-dimethyl) (T_m=255–256°C) and poly(tetramethylene oxide) (PTMO), using a titanium catalyst for the polycondensation, to give high-molecular-weight poly(ether esteramide) segmented copolymers which we abbreviate as T4T-PTMO.

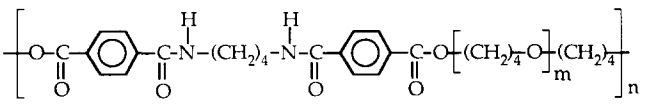

T4T-PTMO

From the data available on bond lengths and angles, and more specifically from those for the related model compound, tetramethylene dibenzamide[12], the length of the hard unit between the ester oxygen atoms in the main chain was calculated to be 1.95 nm. The length of the PTMO segment repeat unit in the extended conformation is estimated to be 0.61 nm. The ester groups are assumed to belong to the hard segment, with the latter thought of as being made up of one repeat unit.

The copolymers all crystallize rapidly, and the temperature dependence of the modulus in the rubber region is low. Although the hard segments were of uniform length, the melting temperatures were found to decrease with increasing soft segment length.

In this work we have analysed the melting behaviour and crystalline structure of these T4T-PTMO segmented copolymers in more detail and have also studied some of their mechanical properties.

EXPERIMENTAL

Materials

The chemical aspects of the synthesis of the segmented copolymers are described in another paper[11]. The PTMO samples had segment lengths with M=250–2900, and are designated as $PTMO_{250}$, etc. in this study.

Differential scanning calorimetry (d.s.c.)

A Perkin-Elmer DSC 7 was used for recording thermograms and for data evaluation, using heating and cooling rates of 20°C min^{-1} and sample weights of 6–17 mg. The thermal analysis procedure adopted was as follows: (i) heating from −100 to 220°C (−80 to 180°C, respectively, in the case of T4T-$PTMO_{2900}$); (ii) equilibration for 5 min at the maximum temperature; (iii) cooling from T_{max} down to −100°C and; (iv) second heating run. The sample cell was kept under nitrogen in order to suppress any degradation of the polymer.

Wide-angle X-ray diffraction (WAXD)

Measurements. A Philips powder diffractometer with a generator operated at 40 kV and 30 mA was used for the WAXD studies; incident radiation was Ni-filtered (CuKα; λ=1.54 nm), and the diffracted radiation was monochromatized. An automatic divergence slit (a.d.s.) was installed, in combination with a receiving slit of 0.1 degree angular divergence at the detector. An angular range from 4 to 60° was scanned with the sample in a reflection geometry arrangement.

The T4T-PTMO copolymers were pressed into films of approximately 1 mm thickness and 33 mm diameter. For the diffractometry experiments they were put on top of a base plate of either Al or Ag and the assembly was clamped into a powder sample holder. In the case of nylon-4,T, a powder sample of 2.4 mm thickness was employed.

Data analysis. Prior data analysis: corrections for the irradiated volume, absorption and polarization were applied to the raw diffraction data. The numerical fitting procedure adopted was that proposed by Heuvel *et al.*[13] for the evaluation of nylon and PET fibre diffraction results. These authors suggested the use of Pearson VII functions:

$$P(x)=P_0/[1+4z^2(2^{1/m}-1)]^m$$

In order to describe the experimental intensity data, several Pearson VII functions are used and combined with an additional baseline:

$$I(x)=Ax+B+\Sigma P_i(x)$$

Pearson VII functions are symmetric around the central coordinate x_0 and contain four parameters: (i) reduced coordinate $z=(x-x_0)/H$; (ii) peak height P_0; (iii) peak width H (f.w.h.m.), and (iv) shape parameter m ($0.5<m<\infty$). The Pearson VII function owes its flexibility to the shape parameter m: for $m=1$ the curve is a Cauchy type, while for $m=\infty$ it is Gaussian.

At least eight Pearson functions were necessary to describe the diffraction patterns of our T4T-PTMO materials in the angular range where 2θ=4–34°, where 2θ is the diffraction angle, and which replaces x in the above equations. A linear baseline was drawn between the intensity data at both ends of this 2θ range. This was necessary in order to strictly separate this angular region from the rest.

Values of the 'crystallite size' (Λ) were determined by means of the Scherrer equation:

$$\Lambda=\frac{\lambda}{\cos(\theta)\,\Delta}$$

which can be expressed by using the parameters of the Pearson VII function as:

$$\Lambda=\frac{\lambda}{\cos\left(\frac{x_0}{2}\right)[H^2-H_G^2]^{1/2}}$$

It is only at this very last stage of the evaluation that we have made corrections for the instrumental and sample broadening effects. The line breadth Δ is calculated from the width parameter H of the Pearson VII function and the geometrical broadening parameter H_G, as shown in the equation above, i.e. under the assumption that all the functions involved have a Gaussian shape. This is obviously not quite correct, since the sample thickness broadening is asymmetric, and the m values of the fitted peaks were found to show a strong variation, although generally $m>1$. Even for the sharper reflections, however, the peak width is four times as large as the width due to the broadening effects.

Small-angle X-ray scattering (SAXS)

SAXS curves were recorded by means of a Kratky camera (Model 1970), equipped with a step scanner. An

entrance slit of 60 μm was used, and the scattering vector $s = 2 \sin \theta / \lambda$ ranged from 0.009 to 0.9 nm^{-1}. Ni-filtered CuKα radiation was generated at 40 kV and 40 mA, and pulse-height discrimination was used in the detector electronics. Samples were cut from the central part of injection moulded tensile dumb-bells, and were ~3 mm in thickness. A Lupolen calibration sample was used for obtaining absolute intensity values.

The data were processed using the program of Vonk[14]. Long period values were calculated from both desmeared Lorentz-corrected data, and from the one-dimensional correlation function. Both procedures are based on the assumption that the scattering originates from stacks of lamellae.

Transmission electron microscopy

A Jeol JEM-200 CX transmission electron microscope, operated at 200 kV, was employed. Small (~1 × 1 × 133 mm) pieces of the injection moulded T4T-PTMO tensile testing samples were repeatedly stained in a 1:1 mixture of 2 wt% aqueous osmium tetroxide solution and 37 wt% formaldehyde solution. The stained material was cryomicrotomed (at −100°C) into sections having a thickness of ⩽100 nm, and were then transferred to Formvar coated copper grids.

Dynamic mechanical thermal analysis (d.m.t.a.)

Torsional tests were carried out on a computer controlled Myrenne torsion pendulum. Compression moulded samples, with dimensions 50 × 9 × 1.8 mm, were dried in vacuum at 110°C for 16 h, prior to testing. The pendulum operated at a frequency of 1 Hz, and the sample was continuously heated from −120°C to the onset of flow, at a rate of 1.8°C min^{-1}.

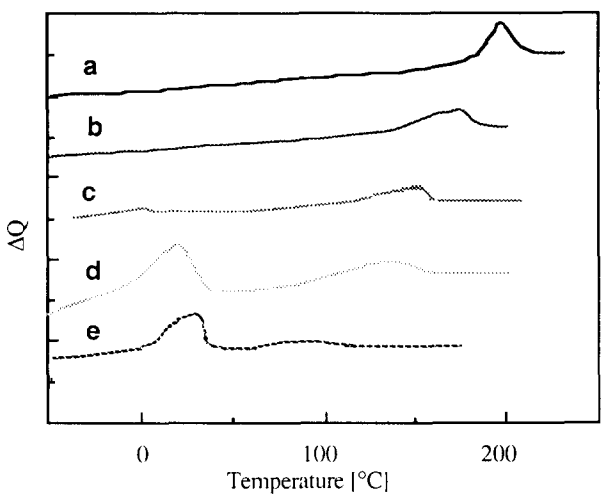

Figure 1 D.s.c. curves of the copolymers: (a) T4T-$PTMO_{250}$; (b) T4T-$PTMO_{650}$; (c) T4T-$PTMO_{1000}$; (d) T4T-$PTMO_{2000}$ and; (e) T4T-$PTMO_{2900}$

Tensile testing

Tensile tests were conducted on an Instron tensile tester. Dumb-bell shaped specimens (described in ISO Recommendations R527 as Type 2 specimens) were employed. Before testing, the specimens were kept dry by storing under vacuum at room temperature. The cross-head speed in the tensile tests was 5 mm min^{-1}. For each polymer, five specimens were strained to break and for at least five of the specimens the Young's modulus was determined using a strain recorder.

RESULTS AND DISCUSSION

Materials

The syntheses of the T4T-PTMO copolymers have been fully described in another paper[11]. The polymers were all opaque and white. T4T-$PTMO_{250}$, which has the shortest soft segment, appeared to be a hard material at room temperature, whereas all of the other samples were rubber-like in nature.

The inherent viscosities were all found to be >0.85 dl g^{-1}, indicating that the polymers had high molecular weights. All samples could be melt processed and their mechanical properties could be studied. The intrinsic viscosities of the polymers are given in *Table 1*. The weight fractions of the hard and soft segments are also given in this table. Since very short hard segments have been built in, very low hard-segment weight fractions are obtained. The mole fractions of the hard segments in the polymers were calculated from the degree of polymerization of the soft segment, by regarding the T4T hard segment as one repeating unit; the hard-segment mole fraction varies from 0.238 to 0.024, with these values being much lower than the values found for commercial segmented block copolymers.

D.s.c. analysis

Melting thermograms of the copolymers are presented in *Figure 1*, with the d.s.c. data given in *Table 1*. In the range −50 to 220°C two first-order transitions can sometimes be found; the high-temperature transition is attributed to the melting of T4T crystals, with the low-temperature transition attributed to the melting of

Table 1 Composition of the copolymers, T4T-$PTMO_M$, and results from d.s.c. measurements

Sample, M^a (g mol^{-1})	$W_h{}^b$	$\eta_{inh}{}^c$ (dl g^{-1})	T_{m_s} (°C)	$\Delta H_s{}^d$ (J g^{-1})	$W_{sc}{}^{d,e}$	$\frac{W_{sc}{}^{d,e}}{W_s}$	T_{m_h} (°C)	ΔT_{m_h} (°C)	ΔH_h (J g^{-1})	$W_{hc}{}^f$	$\frac{W_{hc}{}^f}{W_h}$
250	0.604	1.33	–	0	0	0	185	9	36.2	0.238	0.394
650	0.370	1.39	−33	0	0	0	179	19	28.2	0.185	0.500
1000	0.276	1.18	−13	0	0	0	153	16	27.3	0.179	0.648
2000	0.160	1.49	18	8.3	0.048	0.057	133	11	16.4	0.108	0.675
2900	0.116	0.85	28	23.7	0.138	0.156	84	0	8.7	0.057	0.491

[a] Molar mass of PTMO segment
[b] Weight fraction of T4T segment (including ester groups)
[c] Intrinsic viscosity measured by using a 0.25 g dl^{-1} solution in 1:1 phenol/tetrachloroethane at 25°C
[d] Values based on part of endotherm for which $T > 21$°C
[e] Weight fraction of crystalline soft block
[f] Weight fraction of crystalline hard block

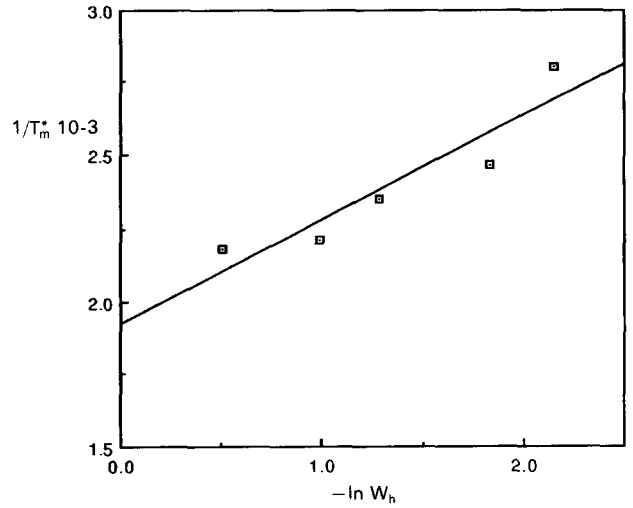

Figure 2 Reciprocal of the melting temperature as a function of the weight fraction of the hard unit in the T4T-PTMO copolymer system

crystalline PTMO. The T4T-PTMO melting temperature decreases with increasing length (or volume fraction) of the soft segments. The melting temperature of a segmented copolymer is considered to be primarily a function of hard segment length, with soft segment length only being of minor importance[2]. Longer hard segments increase the lamellar thickness of the crystallites, and consequently the melting temperature[2]. From another point of view, the melting point of the hard segments is determined by the volume fraction of endgroups to hard units, which becomes smaller with longer hard units[15]. In our thermoplastic elastomers (TPEs), the hard units are supposed to be of uniform length, and consequently melting point differences cannot be attributed to lamellar thickness variations or endgroup-to-segment length ratios. The dependence of the T_m of the hard domains on the soft segment length could originate from a reduced lateral crystallite size or by a 'solvent' effect of the amorphous phase.

The size of the crystallites was found not to be strongly dependent on hard unit concentration, as will be discussed in the section on WAXD analysis (see below). The solvent effect on the melting point of a random copolymer built up from crystallizable A-units and noncrystallizing B-units, has been described by Flory[16] as:

$$\frac{1}{T_m}-\frac{1}{T_m^*}=\left(\frac{R}{\Delta H_f}\right)\ln X_A$$

Here T_m is the observed copolymer melting temperature, T_m^* is the observed melting temperature of the homopolymer A, X_A is the molar fraction of A-units in the copolymer, ΔH_f is the latent heat of fusion of homopolymer A and R is the gas constant. This relationship has been successfully applied by Boussias *et al.*[17] to the melting point depression in random PBT-PTMO segmented copolymers and, more recently, T4T-PTMO segmented copolymers and, more recently, by Takahashi and Nagata[18] for liquid-crystalline polyester-PMTO block copolymers. The mole fractions of these systems are calculated using equal molar volumes of repeat units. The molar volumes of our T4T and PTMO units are not known and thus equal molecular weights for the units were taken. With equal molecular weights the mole fraction X_A and the weight fraction (W_h) are the same.

Our data are plotted as $1/T_m$ vs. $-\ln W_h$ and a linear relationship is obtained (*Figure 2*), with the intercept (at $-\ln W_h=0$) of $1/T_m^*$ at 248°C. This suggests that as long as the lamellar dimensions are not changed the maximum temperature of this system is 248°C.

For these segmented polymers with uniform lengths, the degree of supercooling, ΔT_m ($=T_m-T_c$, see *Table 1*), is very small (9–20°C), in comparison with, for example, a value of 32°C for PBT[19]. As PBT is generally regarded as a fast crystallizing polymer, the supercooling values for the copolymers are, therefore, surprisingly small. The very low ΔT_m value found for T4T-PTMO$_{2900}$ (i.e. 0°C) is due to the low and broad nature of both the melting and crystallization peaks of this polymer, which makes it hard to determine the actual melting and crystallization temperatures (this also holds for the enthalpy values for this polymer). The very low ΔT values suggest order in the melt, but with polarized light microscopy no liquid-crystal polymer (LCP) behaviour could be observed. It is especially worth noting that a large fraction of the hard units crystallizes, even in the copolymers with low concentrations of T4T segments.

From the melt enthalpy values we calculated the weight fractions of the crystalline material that was present. In these calculations a value of 152 J g^{-1} was employed as the melting enthalpy of the T4T units, which is actually the melting enthalpy of the T4T-dimethyl precursor. This value is found to be nearly equal to the value obtained according to the group treatment by Van Krevelen[20], which was 57 kJ per mole of crystalline T4T units (corresponding to 150 J g^{-1}). The values thus obtained for the T4T crystallinity are given in *Table 1* and lie in the range 39–68%.

The low-temperature melting transition originates from the PTMO phase. Soft-segment crystallization is absent for T4T-PTMO$_{250}$, and for the other copolymers it becomes more pronounced with the increasing PTMO segment length (see *Table 1* and *Figure 1*). The soft-segment melting temperature increases with the PTMO segment length (*Figure 3*); longer PTMO segments can, of course, form thicker lamellar crystals, and seem to be less hindered by the hard units and, therefore, are able to form higher-melting crystallites. In T4T-PTMO$_{2000}$ and T4T-PTMO$_{2900}$, crystallization of PTMO can also be enhanced by stretching, as will be discussed later.

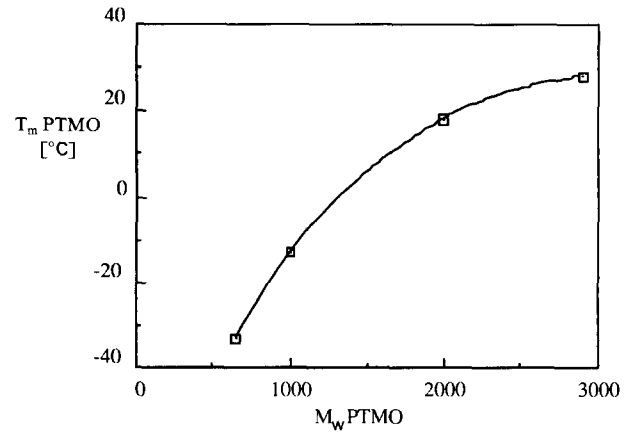

Figure 3 Melting temperatures of the crystalline PTMO fractions as a function of PTMO segment length in the T4T-PTMO copolymer system

Table 2 Composition of the copolymers, T4T-PTMO$_M$

Sample, M	w_a[a]	v_{sc}[b]	v_{hc}[c]	v_a[d]	ρ_a[e] (g cm^{-3})	ρ_{bulk} (g cm^{-3})
250	0.762	0	0.199	0.801	1.143	1.202
650	0.815	0	0.142	0.858	1.050	1.105
1000	0.821	0	0.133	0.867	1.012	1.069
2000	0.844	0.046	0.076	0.878	0.983	1.022
2900	0.805	0.129	0.040	0.831	0.976	1.007

[a] Weight fraction of amorphous component
[b] Volume fraction of crystalline soft block
[c] Volume fraction of crystalline hard block
[d] Volume fraction of amorphous component
[e] Density of the amorphous phase

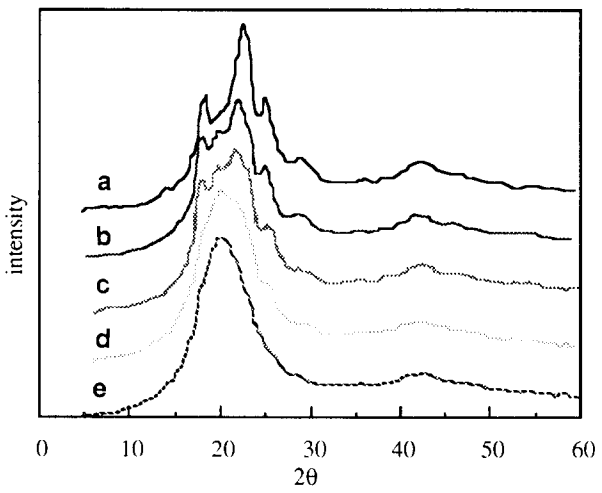

Figure 4 WAXD patterns of the copolymers of: (a) T4T-PTMO$_{250}$; (b) T4T-PTMO$_{650}$; (c) T4T-PTMO$_{1000}$; (d) T4T-PTMO$_{2000}$ and; (e) T4T-PTMO$_{2900}$

For calculation of the PTMO crystallinity, the melting enthalpy value of crystalline PTMO (172 J g^{-1})[21] has been used. As we are interested in the crystalline fraction at room temperature, only the area above 21°C has been taken into account in the endotherm of the d.s.c. thermogram.

Densities

Since the mechanical properties of semicrystalline polymers are generally related to a description of the microstructure in terms of the volume fractions of the various component phases, a knowledge of the density of each phase would be desirable. These data are lacking, however, even for the pure components.

One way to find the densities of the component phases is to start from a three-phase model. In this model (two crystalline phases and a mixed amorphous phase) the weight fractions of the components in the mixed amorphous phase are easily found after the weight fractions of the crystalline phases have been calculated from d.s.c. enthalpy data. The volume fraction of the amorphous phase is then found after the volume fractions of the pure crystalline phases have been assessed by means of their densities. Weight fraction (w), volume fraction (v) and density (ρ) of any phase are related through the bulk density:

$$\rho_i = \frac{w_i \rho_{bulk}}{v_i}$$

and this relationship can be successively applied to all of the phases.

The bulk densities of all of the T4T-PTMO copolymers have been accurately measured by liquid mercury displacement, and the values are listed in *Table 2*. We have carried out a trial optimization in which we have varied the crystalline densities at constant values of the melting enthalpies, in order to simultaneously satisfy the results of small-angle X-ray scattering measurements (to be discussed in a later section). This optimization yielded the following values for the densities of the crystalline phases, i.e. $\rho_{s,c}$ and $\rho_{h,c} = 1.075$ and $1.44\ g\ cm^{-3}$, respectively. These values should be compared with the following, i.e. $\rho_{s,c} = 1.07-1.08\ g\ cm^{-3}$ (ref. 22) and $\rho_{h,c} = 1.46\ g\ cm^{-3}$ (calculated according to Van Krevelen[23]). The volume fractions and densities of the amorphous phase which have been calculated from the optimized values are contained in *Table 2*.

Wide-angle X-ray diffraction

X-ray diffraction experiments were conducted in order to investigate the following:

(i) a possible similarity between the crystalline structure of the hard unit domains and that of nylon-4,T;
(ii) spontaneous and strain-induced PTMO crystallization and;
(iii) the lateral size (i.e. perpendicular to the chain direction) of the hard domains.

The crystal structure of nylon-4,T has not yet been elucidated. We have not been able to produce sufficiently detailed (i.e. oriented) diffraction patterns to carry out assignment of reflections, either for nylon-4,T (solution cast films are brittle and cannot be drawn), or for the copolymers described in this work. The crystallization of PTMO at high strains, suggested by the tensile behaviour of the samples, T4T-PTMO$_{2000}$ and T4T-PTMO$_{2900}$, has been confirmed by WAXD photography. The main reflections of crystalline PTMO, at $2\theta = 20.2°$ and 24.7°[24], show up very strongly in the fibre patterns of drawn samples of both of these copolymers. These reflections do *not* appear for a sample of T4T-PTMO$_{1000}$ drawn to fracture.

WAXD patterns from isotropic samples show rather diffuse rings. Even T4T-PTMO$_{250}$ produces a rather complicated pattern. If any quantitative information is to be obtained from diffraction, numerical accuracy of a diffractometer set-up is required. The copolymers could be conveniently compression moulded into films, suitable for diffraction in reflection geometry, but for nylon-4T, we had to employ a coarse powder sample because it was impossible to process this polymer in the melt. The WAXD patterns are shown in *Figure 4*.

Before using the diffractometer data in the curve-fitting procedure, they were processed as described above in the Experimental section, which gives details of the corrections that were applied to the raw data and to the numerical results of the fitting procedure. The peak positions determined were essentially equal for all five of the samples (*Table 3*). Standard deviations in 2θ were well below 0.1°, except in the case of T4T-PTMO$_{2900}$ where they amounted to several tenths of a degree. Values of 2θ for nylon-4,T are also presented in this table, where it can be seen that the main reflections of the latter are also present in the copolymers, i.e. at 18° and at ~22.4°.

Table 3 Peak positions determined from the WAXD patterns and crystallite sizes Λ calculated from the associated line widths

2θ (°)							
T4T-PTMO	N 4,T copolymer	18.0 17.9	19.6 19.9	22.7 22.2	– 23.3	26.0 25.3	29.1 28.9
Λ (nm)	N 4,T	8.4	–	3.9	–	4.0	–
	T4T-PTMO$_{250}$	7.7	–	4.8	–	5.3	–
	T4T-PMTO$_{650}$	5.9	–	4.3	–	4.4	–
	T4T-PTMO$_{1000}$	6.8	–	3.3	–	4.6	–
	T4T-PTMO$_{2000}$	5.0	–	3.0	–	5.4	–
	T4T-PTMO$_{2900}$	5.5	–	2.4	–	4.1	–

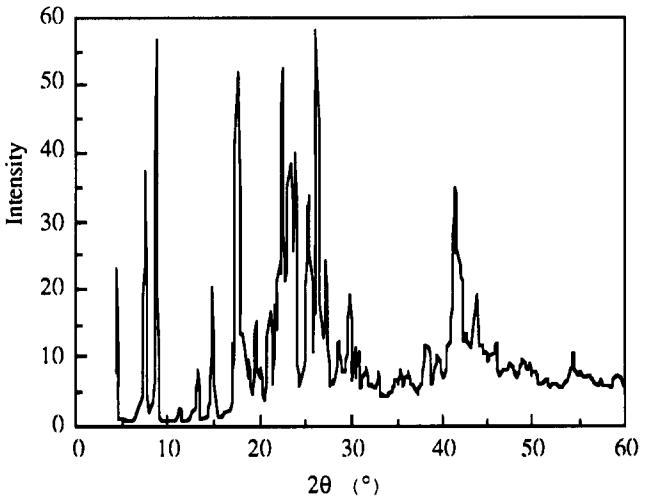

Figure 5 WAXD pattern of the T4T-dimethyl precursor material

The peak at 26° may correspond to that at ~25.3° in the copolymers.

In addition, all our diffraction patterns contain a prominent component at about 20°: a very broad peak ($H \sim 10$) is required here for a good fit to be obtained. This peak is attributed to the amorphous part of the material. Furthermore, the five copolymers show a second peak near $2\theta = 20°$, which is narrower and becomes stronger with increasing PTMO content. Its position corresponds very well to the diffraction angle found for crystalline PTMO homopolymer ($2\theta = 20.2°$). Diffraction in pure PTMO gives rise to a second peak of a similar intensity at 24.7°, for which, however, there is no matching peak in the copolymer patterns. This may be due to the restricted growth of PTMO crystals in a particular direction in the copolymer materials.

The calculated crystal 'sizes' Λ are presented in *Table 3* for nylon-4,T and the T4T-PTMO copolymers. This Λ is a composite quantity which involves both size and microstrain effects. There is not sufficient detail in our diffraction patterns to warrant a more extensive analysis of the peak shapes. The calculated lateral crystal 'size' values are very small, and lie in the range usually encountered for fibrillar crystals. The crystallite dimensions which are associated with the two main reflections decrease slightly with increasing length of the soft segments. We conclude that the variations in crystallite size are too small to have a major effect on the melting temperatures of our T4T-PTMO systems, although we need values for the surface free energies of the crystal faces to substantiate this claim. The Λ-values for nylon-4,T are not particularly large.

Figure 5 shows the diffraction pattern of the precursor material, T4T-dimethyl (see above). This pattern is strikingly more detailed and is typical of low-molar-mass crystalline substances. In the 2θ range between 4 and 34°, approximately 25 diffraction peaks are present, all of them much sharper than any of the T4T-PTMO copolymer peaks. This pattern was not analysed further, but from a comparison of the patterns obtained from different samples of the T4T-dimethyl material, it appears that there is more than one type of crystal structure present. We merely note that the positions of the more intense peaks ($2\theta = 17.5$, 22.5 and 26.3°) correlate rather well with those present in the copolymer patterns, as does the overall intensity distribution (e.g. note the dip beyond $2\theta = 32°$).

To summarize, these X-ray diffraction results indicate similar crystal structures for all of our T4T-PTMO segmented copolymers, and these are not far different from that of nylon-4,T. There is a contribution to the pattern from crystalline PTMO for all of the copolymers, in line with the d.s.c. results. The lateral crystallite 'size' of the hard domains is very small (of the order of 5 nm) and decreases with increasing PTMO content.

Small-angle X-ray scattering

SAXS was used for two reasons: (i) to obtain a characteristic value for the microstructure, i.e. the long period, and; (ii) to assess the validity of the density values for the individual phases. A value for the long period, L, was calculated from both the Lorentz-corrected scattering curve and the one-dimensional correlation function; in both these methods it is implicitly assumed that the microstructure is lamellar in nature. On the basis of the TEM results (see below), this seems to be a reasonable assumption.

The results for T4T-PTMO$_{250}$ are distinct in the sense that two maxima which do not relate to the same periodicity are observed in the Lorentz-corrected, desmeared SAXS curve (*Figure 6*); the correlation function (not shown) is also somewhat irregular. This suggests a non-homogeneous morphology. A WAXD background, to be used in the SAXS data reduction procedure, was determined for the sample T4T-PTMO$_{2900}$ and used thereafter for all five samples. In the harder samples the faint WAXD peak around 7°

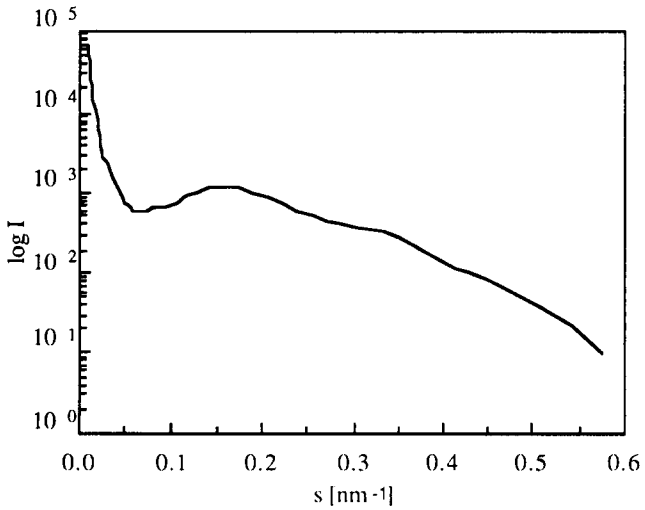

Figure 6 Lorentz-corrected desmeared SAXS curve of the T4T-PTMO$_{250}$ copolymer

Table 4 Results obtained from SAXS measurements on the copolymers, T4T-PTMO$_M$

Sample, M	L_{Lo}[a] (nm)	L_{c1}[b] (nm)	$\overline{\eta^2}$[c] ((mol el cm^3)$^{-2}$)	$\overline{\eta^2}_{calc}$[d] ((mol el cm^3)$^{-2}$)	r[e] (nm)
250	4.9/3.1	5.5	0.0029	0.0029	3.9
650	6.3	6.5	0.0044	0.0039	7.3
1000	8.0	7.5	0.0041	0.0044	10.3
2000	9.4	9.5	0.0028	0.0031	18.7
2900	9.4	9.0	0.0021	0.0020	26.4

[a] Lorentz-corrected long period
[b] Long period from one-dimensional correlation function
[c] Mean-square electron density fluctuation from SAXS experiments
[d] Mean-square electron density fluctuation calculated from the data in *Table 3*
[e] Length of one chain repeat unit

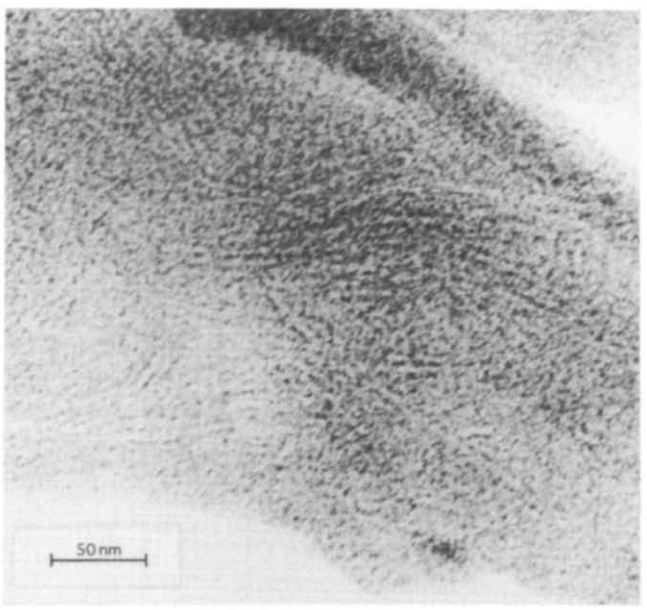

Figure 7 Transmission electron micrograph of the T4T-PTMO$_{250}$ copolymer

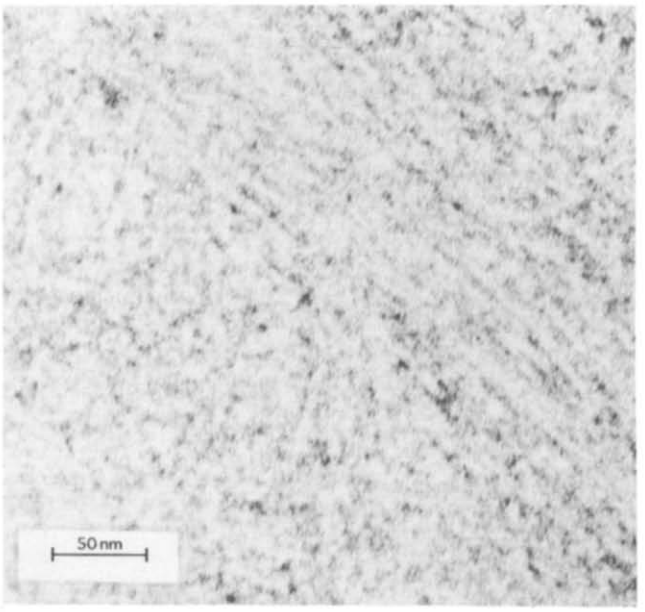

Figure 8 Transmission electron micrograph of the T4T-PTMO$_{650}$ copolymer

becomes more prominent and hampers the determination of the absolute scattering power. This part of the SAXS curve was eliminated by applying a tailfitting procedure to the data. Values of the mean square electron-density fluctuation, $\overline{\eta^2}$, found after tailfitting, are collected in *Table 4*, and compared with values calculated on the basis of a three-phase model. In the latter, the volume fractions and amorphous densities in *Table 2* are used together with the corresponding values for the crystalline densities. The attempted optimization of the density values of the component phases, based on d.s.c., bulk density and SAXS data, in which the three-phase model was used to calculate the small-angle scattering power, is found not to reproduce the abrupt change in the $\overline{\eta^2}$ values that is found between T4T-PTMO$_{250}$ and T4T-PTMO$_{650}$ following from the SAXS data analysis. Therefore, this type of approach, which takes only one amorphous phase into account, appears not to be fully satisfactory.

Although the experimental results for T4T-PTMO$_{250}$ does not indicate any segregation in the amorphous phase, as this would lead to higher $\overline{\eta^2}$ values, it does in fact suggest a more densified amorphous phase.

The last column in *Table 4* lists the length, r, of a chain repeat unit, i.e. the sum of the lengths of the hard and soft segments in an extended conformation. This value was calculated from the number of soft repeat units, and the segment lengths (quoted above in the Introduction). The ratio L/r is higher than 1 for the main SAXS peak in T4T-PTMO$_{250}$, which would imply that not every hard unit is in a crystallite. This is in line with the d.s.c. results (see above), which indicate incomplete crystallization and show an increase in the fraction of crystallized hard units with increasing soft segment length. The ratio L/r becomes smaller with increasing PTMO segment length, which implies that the soft segments are folded in the soft copolymers which are considered here.

Transmission electron microscopy (TEM)

Figures 7 and *8* are transmission electron micrographs of two of our copolymers. Since these materials do not contain unsaturated carbon–carbon bonds, staining was found to be difficult. Various reagents have been tested on the sections, but they resulted in either poor contrast or detail (phosphotungstic acid, methyl iodide, uranyl acetate) or in excessive degradation (RuO_4). The classical OsO_4 method was found to give useful results when applied in the following manner: a bulk specimen suitable for cryomicrotomy (~1 mm diameter) was immersed in a

Table 5 D.m.t.a. data obtained for the copolymers, T4T-PTMO$_M$

Sample, M	T_g (°C)	$G'_{25°C}$ (MPa)	$G'_{100°C}$ (MPa)	T_{flow} (°C)
250	−79, 43	754	201	200
650	−51	116	73	170
1000	−57	65	37	150
2000	−64	18	9.5	135
2900	−65	13	–	95

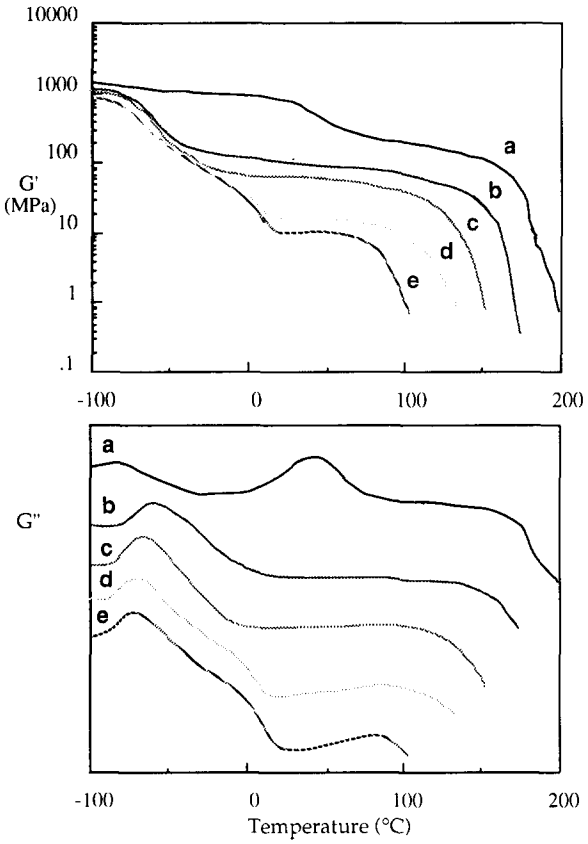

Figure 9 Storage modulus (G') (upper figure) and loss modulus (G'') (lower figure) as a function of temperature for: (a) T4T-PTMO$_{250}$; (b) T4T-PTMO$_{650}$; (c) T4T-PTMO$_{1000}$; (d) T4T-PTMO$_{2000}$ and; (e) T4T-PTMO$_{2900}$

few drops of a liquid consisting of a 1:1 mixture of a 2% aqueous solution of OsO_4 and a 37% aqueous solution of formaldehyde. The liquid was replenished three times in order to intensify the strain. Formaldehyde appears to be absolutely essential for any penetration to occur; it is known to act as a plasticizer for polyamides in general.

The micrographs show that the stain was deposited in a spot-like manner, which hampers the identification of morphological features. However, bundles of lamellae can be detected. In comparing *Figures 7* and *8*, we find that the lamellae look thinner and more closely spaced and the bundles much less isolated in T4T-PTMO$_{250}$ than in T4T-PTMO$_{650}$. This agrees with the small-angle X-ray results, i.e. a shorter period and more detailed diffraction for the T4T-PTMO$_{250}$ material.

We found no indication of a spherulitic superstructure, either during our TEM observations, or in polarization microscopy studies on thicker (5–10 μm) cryosections, which is in contrast with findings made for other TPEs[25,26].

Processing

As far as processing of the powdered polymers by injection moulding is concerned, the remarkaly short cycle time of 25 s at 200°C is worth mentioning (for T4T-PTMO$_{250-2000}$). Only in the case of T4T-PTMO$_{2900}$ was a longer cooling time required (resulting in a total time of 60 s) in order to avoid deformation of the dumb-bell shaped specimens to be used for tensile testing. With the injection moulding machine that was used in these studies, cycle times of ~25 s are also commonly employed for the processing of polyamides and polyamide blends. This is another indication of the high crystallization rates of the hard units in our copolymers, and this conclusion is supported by the low values of supercooling that were found in the d.s.c. experiments.

Torsional modulus analysis

Torsional analysis allows an easy determination of the elastic modulus in the low-strain limit as a function of temperature. In *Table 5* the storage moduli of our copolymers at 25°C and 100°C are listed, with the complete storage and loss modulus curves of the materials displayed in *Figure 9*.

When T4T-PTMO$_{250}$ is compared with the softer materials, the shift of the second-order transition from ~40°C to −60°C is immediately apparent. There is another second-order transition in T4T-PTMO$_{250}$, however, at −79°C, which is more clearly visible in the loss modulus curves of *Figure 9*. The occurrence of two transitions may indicate the presence of two amorphous phases which differ in composition, one being almost pure PTMO (the glass transition of PTMO lies at −84°C), with the other being richer in hard segments. In T4T-PTMO$_{2000}$ and T4T-PTMO$_{2900}$, the start of the rubber plateau is shifted upwards to ~10°C by the appearance of an additional shoulder on the high-temperature side of the glass transition range. In line with the d.s.c. findings, the melting of PTMO crystals is held responsible for this feature, although the d.s.c. endotherm lies at a somewhat higher temperature. The temperature at which flow unambiguously occurs indicates that the d.s.c. endotherms can be related to the melting of the hard domains.

The relationship between the observed glass transition temperature and the molecular weight of the soft segments is shown in *Figure 10*. The steep rise in T_g

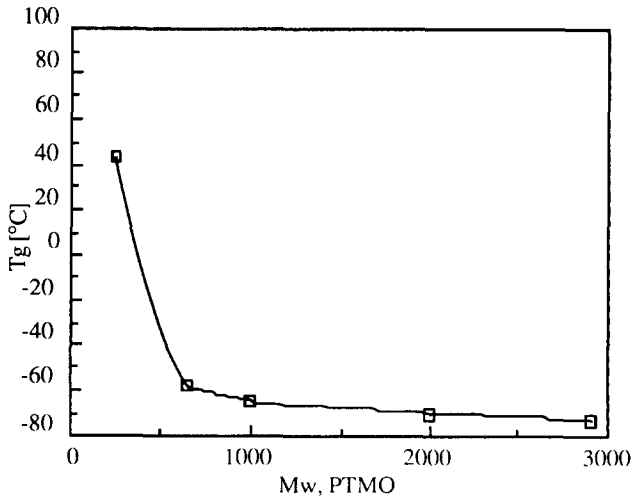

Figure 10 Glass transition temperature as a function of the PTMO segment length in the T4T-PTMO system

Table 6 Tensile data obtained for the copolymers, T4T-PTMO$_M$

Sample, M	E (MPa)	σ_{yield} (MPa)	ε_{yield} (%)	σ_{break} (MPa)	ε_{break} (%)
250	1200	–	–	24.9	6.3
650	265	15.4	36.7	22.7	800
1000	137	10.5	90.4	11.7	510
2000	44	5.4	148	18.1	1450
2900	33	3.6	130	>24	1250

between PTMO$_{650}$ and PTMO$_{250}$ could be due to the reduced mobility of a short chain in between crystalline segments. The theoretical T_g of the T4T component, calculated by Van Krevelen's method[27], is 166°C, which appears to be a reasonable value for the intercept where $M_{PTMO}=0$.

Stress–strain analysis

The five samples show strikingly different drawing behaviour (see *Table 6* and *Figure 11*). T4T-PTMO$_{250}$ shows fracture without yielding at very low strain, while the other samples show yielding. For T4T-PTMO$_{650}$ and T4T-PTMO$_{1000}$ the stress reaches a plateau level, whereas T4T-PTMO$_{2000}$ and T4T-PTMO$_{2900}$ are much more elastomeric in character, showing very low initial moduli, a sigmoidal curve and a strain at break exceeding 1000%. The final breaking stress is several times as large as the stress at the inflection point, and the overall behaviour is attributable to strain-induced crystallization, similar to that occurring in natural rubber.

As has been discussed previously, X-ray diffraction unequivocally shows that PTMO crystallization occurs in samples of T4T-PTMO$_{2000}$ and T4T-PTMO$_{2900}$ during stretching. The samples T4T-PTMO$_{650}$ and T4T-PTMO$_{1000}$ when drawn to fracture do not show any sign of induced PTMO crystallization in WAXD studies, although in drawing T4T-PTMO$_{650}$ the stress rises again after the yield plateau. In this case, the crystallization may be transient and might disappear again upon unloading at fracture. Only relaxed samples have so far been investigated by means of X-ray diffraction while the relaxation behaviour is subject to further study.

CONCLUSIONS

Segmented copolymers of the type T4T-PTMO, which contain crystallizable T4T-units of uniform length, crystallize very fast and have a high crystallinity. The melting temperature was found to decrease with increasing PTMO segment length. This effect was not due to a change in lamellar thickness or width and could best be explained as being due to a 'solvent' effect of the PTMO segment. The very fast crystallization of these materials suggests an ordering of the T4T-units in the melt. LCP behaviour was, however, not observed. The T_g increased with decreasing length of the PTMO segments. The mobility of short PTMO segments ($M=250$) seems to be strongly hindered by the T4T-units. The modulus of the polymers ranged from very hard to very soft, depending on the length of the PTMO segments, and the modulus of the copolymers above the T_g was found to be almost independent of temperature, which is a characteristic of a uniform segment-length system. The materials with PTMO lengths of 650 and over showed typical TPE behaviour with high elongations at break.

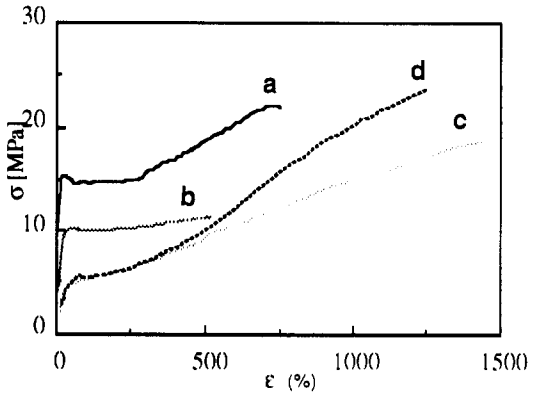

Figure 11 Stress–strain curves of the copolymers: (a) T4T-PTMO$_{650}$; (b) T4T-PTMO$_{1000}$; (c) T4T-PTMO$_{2000}$ and; (d) T4T-PTMO$_{2900}$

ACKNOWLEDGEMENTS

This work is part of the IOP–PCBP research programme. The authors would like to express their gratitude to Mrs ir. J. L. de Haan for her help in the synthesis, Mr J. Boeysma for carrying out the X-ray diffraction experiments, Dr M. Kunz (University of Freiburg, Germany) for help in the electron microscopy studies and Mr H. Mannee (Akzo, Arnhem) for making the X-ray profile analysis program available to us.

REFERENCES

1 'Thermoplastic Elastomers - A Comprehensive Review' (Eds N. R. Legge, G. Holden and H. E. Schroeder), Hanser, Munich, 1987
2 Adams, R. K. and Hoeschele, G. K. in 'Thermoplastic Elastomers – A Comprehensive Review' (Eds N. R. Legge, G. Holden and H. E. Schroeder), Hanser, Munich, 1987, Ch. 8, p. 47
3 Meckel, W., Goyert, W. and Wieder, W. in 'Thermoplastic Elastomers – A Comprehensive Review' (Eds N. R. Legge, G. Holden and H. E. Schroeder), Hanser, Munich, 1987, Ch. 2, p. 3
4 Deleens, G. in 'Thermoplastic Elastomers – A Comprehensive Review' (Eds N. R. Legge, G. Holden and H. E. Schroeder), Hanser, Munich, 1987, Ch. 9B, p. 215
5 Van Hutten, P. F., Walch, E., Veeken, A. H. M. and Gaymans, R. J. *Polymer* 1990, **31**, 524
6 Nelb, R. G., Chen, A. T. and Onder, K. in 'Thermoplastic Elastomers – A Comprehensive Review' (Eds N. R. Legge, G. Holden and H. E. Schroeder), Hanser, Munich, 1987, Ch. 9A, p. 197
7 Ng, H. N., Allegrezza, A. E., Seymour, R. W. and Cooper, S. L. *Polymer* 1973, **14**, 255
8 Harrell, L. L. *Macromolecules* 1969, **2**, 607
9 Miller, J. A., Lin, S. B., Hwang, K. K. S, Wu, K. S., Gibson, P. E. and Cooper, S. L. *Macromolecules* 1985, **18**, 32
10 Eisenbach, C. D., Baumgartner, M. and Günter, G. in 'Advances in Elastomer and Rubber Elasticity' (Eds J. Lal and J. E. Mark), Plenum, New York, 1987, p. 51
11 Gaymans, R. J. and de Haan, J. L. *Polymer* in press
12 Harkema, S., van Hummel, G. J. and Gaymans, R. J. *Acta Crystallogr., Sect. B* 1980, **36**, 3182
13 Heuvel, H. M., Huisman, R. and Lind, K. C. J. B. *J. Polym. Sci., Polym. Phys. Edn* 1976, **14**, 921
14 Vonk, C. G. *J. Appl. Crystallogr.* 1975, **8**, 340
15 Wegner, G. in 'Thermoplastic Elastomers – A Comprehensive Review' (Eds N. R. Legge, G. Holden and H. E. Schroeder), Hanser, Munich, 1987, Ch. 12, Section 5, p. 405

16 Flory, P. J. *Trans. Faraday Soc.* 1955, **51**, 848
17 Boussias, C. M., Peters, R. H. and Still, R. H. *J. Appl. Polym. Sci.* 1980, **25**, 855
18 Takahashi, T. and Nagata, F. *J. Macromol. Sci. Phys.* 1991, **30**, 25
19 Manuel, H. J. and Gaymans, R. J. *Polymer* 1933, **34**, 636
20 Van Krevelen, D. W. 'Properties of Polymers', Elsevier, Amsterdam, 1989, Ch. 5B, p. 118
21 Hreutz, M., Meurer, B., Lotz, B. and Weilk, G. *J. Polym. Sci., Polym. Phys. Edn* 1988, **26**, 663
22 Dreyfuss, P., Dreyfuss, M. P. and Pruckmayr, G. in 'Encyclopedia of Polymer Science and Engineering' (Eds H. F. Mark, N. M. Bikales, C. G. Overberger and G. Menges), 2nd Edn, Vol. 16, Wiley, New York, 1989, p. 649
23 Van Krevelen, D. W. 'Properties of Polymers', Elsevier, Amsterdam, 1989, Ch. 4B, p. 76
24 Hwang, K. K. S., Hemker, D. J. and Cooper, S. L. *Macromolecules* 1984, **17**, 307
25 Seymour, R. W., Overton, J. R. and Corley, L. S. *Macromolecules* 1975, **8**, 331
26 Zhu, L. and Wegner, G. *Makromol. Chem.* 1981, **182**, 3625
27 Van Krevelen, D. W. 'Properties of Polymers', Elsevier, Amsterdam, 1989, Ch. 6A, p. 130